IMPROVED FUNCTIONAL CORTICAL PARCELLATION USING A NEIGHBORHOOD-INFORMATION-EMBEDDED AFFINITY MATRIX

Chendi Wang, Burak Yoldemir, Rafeef Abugharbieh

Biomedical Signal and Image Computing Lab, The University of British Columbia, Canada

ABSTRACT

Cortical parcellation of the human brain typically serves as a basis for higher-level analyses such as connectivity analysis and investigation of brain network properties. Inferences drawn from such analyses can be significantly confounded if the brain parcels are inaccurate. In this paper, we propose a novel affinity matrix structure based on multiple kernel density estimation for cortical parcellation. Neighborhood functional connectivity is embedded into the affinity matrix, which serves the dual purpose of allowing self-adaptive adjustment of voxel affinity values and providing robustness against noise. The proposed affinity matrix can be used with any parcellation method that takes an affinity matrix as its input. In our validation tests, we apply normalized cuts on our proposed affinity matrix to evaluate performance. On synthetic and real data, we demonstrate that the use of our proposed affinity matrix in lieu of the classical definition better delineates spatially contiguous parcels with higher test-retest reliability and improved inter-subject consistency.

Index Terms **—** Affinity matrix, clustering, functional cortical parcellation, neighborhood connectivity.

1. INTRODUCTION

Parcellating the brain through subdivision of the cerebral cortex into sub-units that are internally homogeneous in certain aspects is a challenging problem. Parcellation typically forms the basis for higher-level tasks such as connectivity analysis in diseased populations and analysis of brain network properties [1]. These endeavors can be greatly confounded if true brain parcels are not captured. To investigate brain function, delineation of functionally distinct areas, as opposed to traditional anatomy-based descriptions such as Brodmann areas, is of particular interest [2]. To this end, functional brain parcellation based on functional magnetic resonance imaging (fMRI) data has been gaining increasing popularity in recent years [3].

With no ground truth available, various unsupervised clustering methods have been employed for functional parcellation [2], including independent component analysis, Gaussian mixture model (GMM), k-means clustering and its fuzzy alternative, hierarchical clustering methods [3], region growing [2], graph-based methods such as normalized cuts (Ncuts) [4]. The majority of these parcellation approaches rely on calculating an affinity matrix that encodes the functional similarity between image voxels. As such, defining an affinity matrix that accurately represents the underlying structure is central in clustering applications.

In this paper, we propose a novel affinity matrix constructed using a Gaussian kernel with self-adaptive density estimation instead of the classical fixed density approach. We accomplish this by embedding local neighborhood information into the affinity matrix while making a distinction between voxels at parcel boundaries and those in interior regions. Our rationale is that, being the sole input to most clustering methods, affinity matrices should encapsulate as much relevant information as possible, rather than just average statistical dependencies of the observed time series as is commonly used [5]. The advantages of our method are two-fold: First, the distinction between voxels at boundaries and those in interior regions helps preclude pooling information from different parcels, which would result in ambiguous affinity values. Second, such distinction enables emphasizing or de-emphasizing the affinity values based on putative cluster memberships of voxels, ameliorating the adverse effects of noise.

To evaluate our proposed approach, we apply Ncuts to both synthetic and real data using the classical and proposed modified affinity matrix. We opt to use Ncuts since it has been shown to outperform GMM [2]. Furthermore, Ncuts is relatively insensitive to seed initialization unlike k-means algorithm. However, it is important to note that our proposed affinity matrix can be used in conjunction with any parcellation method that operates on affinity matrices. On synthetic data, we show that higher parcellation accuracy can be attained with our modification of the classical affinity matrix. On real data obtained from Human Connectome Project (HCP) [6], we show that our method exhibits higher test-retest reliability and improved inter-subject consistency.

2. METHODS

2.1. Notation and Background

Let $\mathbf{Z}$ be a $t \times d$ matrix of pre-processed time courses, where t is the number of time points and d is the number of voxels.

We start by estimating the functional connectivity (FC) matrix using Pearson's correlation: $\mathbf{C}=\mathbf{Z}^{\mathrm{T}}\mathbf{Z}/(t\text{-}1)$. Interpretation of negative correlations is currently an open problem, however, it appears that negative correlations are not grounded in strong structural connectivity unlike positive correlations [7]. We thus set negative values in **C** to zero. Traditionally, correlations are mapped using a Gaussian kernel to generate an affinity matrix for clustering as in (1):

$$\mathbf{A}_{ij} = \exp(-\frac{d_{ij}^2}{2\sigma^2}) \quad (1)$$

where d_{ij} is the distance between voxels i and j, which we set to be $1\text{-}\mathbf{C}_{ij}$, and σ is a parameter controlling how rapidly $\mathbf{A}_{ij}$ decays with increasing distance. Usually, σ is set to be the average distance among neighboring voxels over the whole affinity matrix [3]. This classical affinity matrix as given in (1) assumes a fixed density distribution, which rarely holds in practice. To adaptively tune σ based on local statistics of voxel neighborhoods, (1) has been modified as below [8]:

$$\mathbf{A}_{ij} = \exp(-\frac{d_{ij}^2}{\sigma_i\sigma_j}) \quad (2)$$

where σ_i and σ_j are *local* scaling parameters. Based on empirical observations, Zelnik et al. suggested that setting σ_i to be the distance between voxel i and its 7^{th} nearest neighbor outperforms the fixed density kernel [8]. In the sequel, we refer to the fixed density method in (1) as FD, and multiple density method in (2) as MD.

Using FD or MD along with an unsupervised clustering method typically results in parcels that are not contiguous, which contrasts the typical definition of a parcel [4]. A simple spatial constraint that ensures spatial contiguity of voxels involves modifying **A** as follows:

$$\mathbf{A}_{ij} = \begin{cases} \mathbf{A}_{ij}, & D_{ij} \le 1 \\ 0, & D_{ij} > 1 \end{cases}, \quad D_{ij} = \max(|\,(x_i, y_i, z_i) - (x_j, y_j, z_j)\,|) \quad (3)$$

where (x_i, y_i, z_i) and (x_j, y_j, z_j) are the 3D coordinates of voxels i and j, respectively [4]. With this constraint, each voxel is allowed to only connect to its immediate neighbors prohibiting parcels with spatially distributed voxels.

In this work, we propose a novel affinity matrix that builds upon MD. We describe our improved kernel density estimation strategy in Section 2.2. We further refine the affinity values by incorporating local neighborhood information as given in Section 2.3.

2.2. Multiple Density Kernel Scaling

Although MD kernel has been proven to outperform the classical Gaussian kernel [8], we argue that the choice of local scaling parameter σ_i is vulnerable to noise. Instead, we set σ_i to be the average distance between voxel i and the voxels within its neighborhood in the same cluster. This is a non-trivial task given that the clustering structure of the data is unknown at this stage. To this end, we use cues from the regular grid structure of the voxels to construct a rule of thumb. Essentially, each voxel in a cluster can be classified as either a boundary point (BP) or an interior point (IP). The neighbors of the former have a heterogeneous cluster membership structure whereas all neighbors of the latter belong to the same cluster. For illustration, a 2D example of a BP is given in Fig. 1. The center voxel outlined in red can have up to seven neighbors not belonging to its own cluster. Among these cases, the ratio of the number of voxels in the same cluster as the center voxel divided by the total number of the neighbors ranges from 7/8 to 1/8. At least one fourth of the neighbors of a given voxel tend to be in the same cluster in practice. Similar observations hold for the 3D case. Since voxels within the same cluster should have shorter distances compared to those in different clusters, we assume that nearest one fourth of a voxel's neighbors should almost always be in the same cluster with the given voxel. Among these neighbors, we discard the closest and furthest neighbors as possible outliers and estimate σ_i as $\overline{d_i}$, the average distance of remaining voxels.

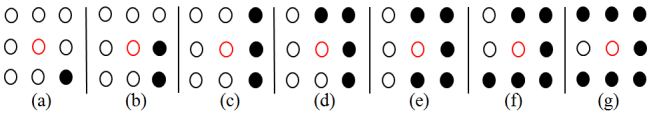

Fig. 1. Some of the possible BP distributions for the center voxel outlined in red. Black and white represent different cluster labels.

2.3. Neighborhood Information

Based on the likelihood of whether two voxels belong to the same cluster or not, we can further modify the affinity values to accentuate the difference between intra-cluster and inter-cluster affinity values. Denoting the distances between voxel i and its neighbors as $\{d_i\}$, the values below the 30^{th} percentile of $\{d_i\}$ as $\{d_i\}_{\mathrm{S}}$, and the values above the 70^{th} percentile of $\{d_i\}$ as $\{d_i\}_{\mathrm{L}}$, we introduce a parameter K as an indicator of the spread of the distance values in the neighborhood of voxel i:

$$K_i = L_i - S_i \quad (4)$$

where L_i and S_i are the median values of $\{d_i\}_{\mathrm{L}}$ and $\{d_i\}_{\mathrm{S}}$. Intuitively, K_i is small when voxel i is an IP, and large when voxel i is a BP, since the spread of $\{d_i\}$ will be larger if voxel i has neighbors from different clusters. With this definition, which indirectly allows us to distinguish between IPs and BPs, we define our affinity matrix as neighborhood-information-embedded multiple density kernel (NMD):

$$\mathbf{A}_{ij} = \exp(-\frac{K_i K_j d_{ij}^{\,2}}{\overline{d_i}\,\overline{d_j}}). \quad (5)$$

This effectively modifies the $\mathbf{A}_{ij}$ values based on the cluster memberships of voxels i and j. Specifically, it scales $\mathbf{A}_{ij}$ up when i and j are in the same cluster, and scales it down when they are not. If two *neighboring* voxels i and j belong to different clusters, they then must both be BPs. In this case, d_{ij} is large and large K_iK_j makes the numerator of the exponential function in (5) larger than in (2), scaling

down $\mathbf{A}_{ij}$. In noisy cases, an adverse effect of noise is that d_{ij} might decrease. However, K_i and K_j are still large, which suppresses the noise by keeping $\mathbf{A}_{ij}$ relatively small. The opposite holds if i and j belong to the same cluster. In this case, either both i and j are IPs, or one of them is a BP. This will lead to a relatively small K_iK_j, scaling up $\mathbf{A}_{ij}$. In case that noise increases d_{ij}, K_iK_j mitigates the effect of noise by keeping relatively large $\mathbf{A}_{ij}$.

3. MATERIALS

3.1. Synthetic Data

For quantitative validation on synthetic data, we simulated a dataset comprising six horizontally connected clusters on a 3D grid of 5×5×30 voxels, with each cluster comprising a cubic region of 5×5×5 voxels. Based on this configuration of voxels, we generated a binary $n \times n$ ground truth affinity matrix, where n=750 is the total number of voxels. For each voxel, we simulated time courses by randomly drawing samples from a multivariate normal distribution with zero mean and covariance structure given by the affinity matrix of the data. We added Gaussian noise to the time courses with the signal to noise ratio set to -10 dB. This noise level was deliberately chosen to be very low to assess the robustness of our method under severe noise conditions. We repeated this process generating 50 noisy versions of the ground truth.

3.2. Real Data

For validation on real data, we used resting-state fMRI (RS-fMRI) data of M=38 healthy adults (17 males and 21 females) with ages ranging from 22 to 35 from the HCP Q2 data release [6]. As advised by the HCP, two subjects with structural abnormalities in the original dataset were excluded. The dataset comprised two sessions of RS-fMRI scans, each having 30 minute acquisitions with a TR of 0.72 s and a voxel size of 2 mm (isotropic). In addition to the minimal preprocessing already applied to the data by HCP [9], we regressed out motion artifacts, mean white matter and cerebrospinal fluid signals, and principal components of high variance voxels found using CompCor [10]. Finally, a bandpass filter with cutoff frequencies of 0.01 and 0.1 Hz was applied. In this work, we focused on functionally subdividing the inferior parietal lobule (IPL) and cingulate cortex (Cg), which possess functional and anatomical heterogeneity [11, 12]. We masked the voxels within IPL and Cg using automated anatomical labeling (AAL) atlas.

4. RESULTS AND DISCUSSION

4.1. Synthetic Data

We evaluated our proposed method by comparing the results of applying Ncuts on (2) and (5). We estimated six clusters from each of the 50 noisy synthetic datasets. We compared the identified clusters to the ground truth using two performance metrics: the Dice similarity coefficient (DICE) [13] and the adjusted Rand index (ARI) [3]. Both metrics range between 0-1, and higher values correspond to better matching between two sets of clusters. Over the 50 synthetic datasets, the average performance as assessed by DICE was found to be 0.91±0.04 when (2) was used. With the proposed affinity matrix in (5), the performance increased to 0.94±0.041. For ARI, the use of (5) instead of (2) increased the average performance from 0.83±0.05 to 0.88±0.07. The difference between the performances obtained using (2) and (5) was statistically significant at $p<0.02$ based on paired-sample t-test for both metrics. (All sequent p values are based on paired-sample t-test).

4.2. Real Data

Cortical parcellations are notoriously difficult to validate due to the lack of ground truth. However, assuming there truly is a functional parcellation, it should presumably remain stable for each subject and consistent across subjects [1]. Thus, to measure the performance of parcellation we quantify its reproducibility using DICE and ARI. In this study, we focus on parcellating IPL and Cg and defer whole-brain parcellation for future work. As commonly suggested in the literature [11, 12], we divide the IPL and Cg into six and nine subregions in our experiments, respectively.

4.2.1. Within-subject test-retest reliability

To evaluate the test-retest reliability of our proposed approach, we calculated the subject-specific parcellation maps from the two RS-fMRI sessions of each subject separately. We then compared the resulting two parcellation maps for each subject, and averaged the results across subjects. The results are statistically significantly higher with our proposed affinity matrix (5) than with (2) at $p<0.02$, using both DICE and ARI, as shown in Table 1.

Table 1. Mean Dice and ARI score ± SE in IPL and Cg

IPL			Cg		
	Eq. (2)	**Proposed**		**Eq. (2)**	**Proposed**
DICE	**0.91±0.04**	**0.95±0.03**	**DICE**	**0.95±0.02**	**0.98±0.01**
ARI	**0.83±0.06**	**0.88±0.05**	**ARI**	**0.91±0.03**	**0.97±0.03**

4.2.2. Inter-subject consistency

We adopted a leave-one-out cross-validation approach to assess inter-subject consistency. Taking one subject at a time, we compared the group parcellation map obtained using the remaining M-1 subjects with the subject-specific parcellation map. For generating group parcellation maps, we averaged the subject-specific affinity matrices prior to applying Ncuts. On average, in IPL, using (5) instead of (2) resulted in an improvement of 0.07 in DICE and 0.11 in ARI. In Cg, the improvement was 0.06 in DICE and 0.12 in ARI. For both metrics, the difference is statistically significant at $p<0.002$. The results are presented in Fig. 2.

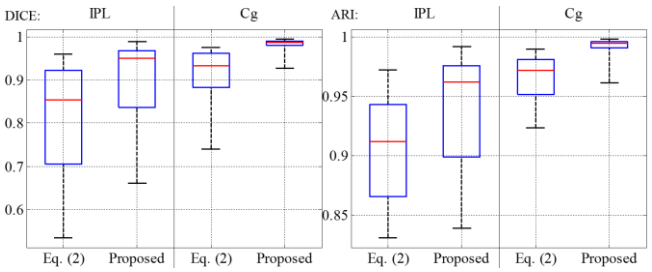

Fig. 2. Inter-subject consistency quantified using DICE (left) and ARI (right) in IPL and Cg for the HCP data. Eq. (2) refers to using (2), and proposed refers to using our proposed affinity matrix in (5) for parcellation. As reflected in the box plots, our method consistently outperforms using (2). The blue rectangle spans the first quartile to third quartile. The red line indicates the median and the black whiskers indicate the minimum and maximum.

4.2.3. Qualitative results

To qualitatively assess the reliability of our proposed method, we generated a group parcellation map by applying Ncuts to the average affinity matrix of all M subjects, and compared it with the subject-specific parcellation maps. For brevity, we only present subjects showing the highest and lowest agreement with the group map as measured by DICE in Fig. 3. The group maps obtained using equation (2) and proposed affinity matrices did not exhibit major differences implying that using (2) for parcellation suffices when there is enough data. However, the subject-specific map having the lowest DICE (top right) with the group map shows major differences compared to the group map (top left) when (2) is used. Specifically, both the number of parcels in the slice shown and the parcel boundaries are significantly different. In contrast, using our proposed affinity matrix results in much more consistent results.

5. CONCLUSIONS

We proposed a novel affinity matrix structure for brain cortex parcellation based on multiple kernel density distribution estimation. Our approach can be used in conjunction with any parcellation method that takes an affinity matrix as its input. On synthetic data, we illustrated that our proposed affinity matrix (NMD) in equation (5) can better represent the data structure by capturing neighborhood functional connectivity leading to more accurate results compared to the multiple density affinity matrix (MD) in equation (2). On real RS-fMRI data from 38 HCP subjects, we demonstrated the superiority of our method in terms of better test-retest reliability and higher inter-subject consistency. Qualitatively, we showed that subject-specific parcellation maps better resemble the group maps when parcellating using our affinity matrix. Our future work will focus on extension to whole-brain parcellation and automatic selection of the number of clusters.

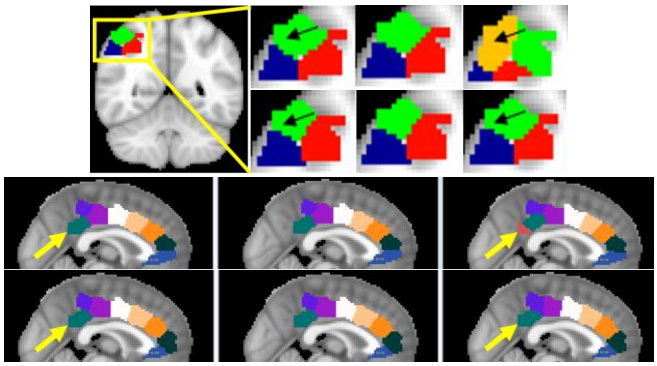

Fig. 3. Qualitative parcellation results for IPL and Cg using the HCP data. In each area - Top: Using the MD in (2); Bottom: Using our proposed affinity matrix NMD in (5). The 1st column shows the group maps while the 2nd and 3rd columns are the subject-specific maps with the highest and lowest DICE with group maps, respectively. The significant differences between the subject-specific map having the lowest DICE (right) and the group map (left) are highlighted with arrows.

6. REFERENCES

[1] X. Shen, et al., "Graph-theory based parcellation of functional subunits in the brain from resting-state fMRI data," *Neuroimage*, vol. 50, no. 3, pp. 1027-1035, 2010.

[2] B. Thomas, et al., "Spatially constrained hierarchical parcellation of the brain with resting-state fMRI," *Neuroimage*, vol. 76, pp. 313-324, 2013.

[3] B. Thirion, et al. "Which fMRI clustering gives good brain parcellations?" *Frontiers in Neuroscience*, vol. 8, no. 167, 2014.

[4] R. C. Craddock, et al., "A whole brain fMRI atlas generated via spatially constrained spectral clustering," *Human brain mapping*, vol. 33, no. 8, pp. 1914-1928, 2012.

[5] S. M. Smith, et al., "Network modelling methods for FMRI," *Neuroimage*, vol. 54, no.2, pp. 875-891, 2011.

[6] D.C. Van Essen, et al., "The WU-Minn Human Connectome Project: An overview," *NeuroImage*, vol. 80, pp. 62-79, 2013.

[7] P. Skudlarski, et al., "Measuring brain connectivity: Diffusion tensor imaging validates resting state temporal correlations," NeuroImage, vol. 43, no. 3, pp. 554-561, 2008.

[8] M. Zelnik, et al., "Self-tuning spectral clustering," *Advances in neural information processing systems*, pp. 1601-1608, 2004.

[9] M. F. Glasser, et al., "The minimal preprocessing pipelines for the Human Connectome Project," *Neuroimage*, vol. 80, pp. 105-124, 2013.

[10] Y. Behzadi, et al., "A component based noise correction method (CompCor) for BOLD and perfusion based fMRI," *Neuroimage*, vol. 37, no. 1, pp. 90-101, 2007.

[11] J. Wang, et al., "Tractography based parcellation of the human left inferior parietal lobule," *Neuroimage*, vol. 63, no. 2, pp. 641-652, 2012.

[12] C. Yu, et al., "Functional segregation of the human cingulate cortex is confirmed by functional connectivity based neuroanatomical parcellation," *Neuroimage*, vol. 54, no.4, pp. 2571-2581, 2011.

[13] L.R. Dice, "Measures of the Amount of Ecologic Association Between Species," *Ecology*, vol. 26, no. 3, pp. 297-302, 1945.